

Probing the interstellar medium and star formation of the Most Luminous Quasar at $z=6.3$

Ran Wang¹, Xue-Bing Wu^{1,2}, Roberto Neri³, Xiaohui Fan^{4,1}, Fabian Walter⁵, Chris L. Carilli⁶, Emmanuel Momjian⁶, Frank Bertoldi⁷, Michael A. Strauss⁸, Qiong Li², Feige Wang², Dominik A. Riechers⁹, Linhua Jiang¹, Alain Omont¹⁰, Jeff Wagg¹¹, Pierre Cox¹²

ABSTRACT

We report new IRAM/PdBI, JCMT/SCUBA-2, and VLA observations of the ultraluminous quasar SDSSJ010013.02+280225.8 (hereafter, J0100+2802) at $z=6.3$, which hosts the most massive supermassive black hole (SMBH) of $1.24 \times 10^{10} M_{\odot}$ known at $z>6$. We detect the [C II] $158\mu\text{m}$ fine structure line and molecular CO(6-5) line and continuum emission at 353 GHz, 260 GHz, and 3 GHz from this quasar. The CO(2-1) line and the underlying continuum at 32 GHz are also marginally detected. The [C II] and CO detections suggest active star formation and highly excited molecular gas in the quasar host galaxy. The redshift determined with the [C II] and CO lines shows a velocity offset of $\sim 1000 \text{ km s}^{-1}$ from that measured with the quasar Mg II line. The CO (2-1) line luminosity provides direct constraint on the molecular gas mass which is about

¹Kavli Institute of Astronomy and Astrophysics at Peking University, No.5 Yiheyuan Road, Haidian District, Beijing, 100871, China

²Department of Astronomy, School of Physics, Peking University, No. 5 Yiheyuan Road, Haidian District, Beijing, 100871, China

³Institute de Radioastronomie Millimetrique, St. Martin d’Heres, F-38406, France

⁴Steward Observatory, University of Arizona, 933 N Cherry Ave., Tucson, AZ, 85721, USA

⁵Max-Planck-Institute for Astronomy, Königsstuhl 17, 69117 Heidelberg, Germany

⁶National Radio Astronomy Observatory, PO Box 0, Socorro, NM, USA 87801

⁷Argelander-Institut für Astronomie, University of Bonn, Auf dem Hügel 71, 53121 Bonn, Germany

⁸Department of Astrophysical Sciences, Princeton University, Princeton, NJ, USA, 08544

⁹Astronomy Department, Cornell University, 220 Space Sciences Building, Ithaca, NY 14853, USA

¹⁰Institut d’Astrophysique de Paris, UMR 7095, CNRS and Universite Pierre et Marie Curie, Paris, France

¹¹Square Kilometre Array Organisation, Jodrell Bank Observatory, Jodrell Bank, Macclesfield SK11 9DL

¹²Joint ALMA Observatory, Alonso de Córdova 3107, Vitacura, Santi-ago, Chile

$(1.0 \pm 0.3) \times 10^{10} M_{\odot}$. We estimate the FIR luminosity to be $(3.5 \pm 0.7) \times 10^{12} L_{\odot}$, and the UV-to-FIR spectral energy distribution of J0100+2802 is consistent with the templates of the local optically luminous quasars. The derived [C II]-to-FIR luminosity ratio of J0100+2802 is 0.0010 ± 0.0002 , which is slightly higher than the values of the most FIR luminous quasars at $z \sim 6$. We investigate the constraint on the host galaxy dynamical mass of J0100+2802 based on the [C II] line spectrum. It is likely that this ultraluminous quasar lies above the local SMBH-galaxy mass relationship, unless we are viewing the system at a small inclination angle.

Subject headings: galaxies: starburst — galaxies: evolution — galaxies: high-redshift — quasars: individual (SDSS J010013.02+280225.8)

1. Introduction

An ultraluminous quasar, SDSS J010013.02+280225.8 (hereafter, J0100+2802) with a bolometric luminosity of $L_{\text{bol}} = 4.3 \times 10^{14} L_{\odot}$ and a supermassive black hole (SMBH) mass of $M_{\text{BH}} \approx 1.2 \times 10^{10} M_{\odot}$, was discovered at $z=6.3$ (Wu et al. 2015). This is by far the most optically luminous object, with the most massive SMBH, among the ~ 50 quasars known at $z > 6$ (Fan et al. 2006; Willott et al. 2010; Jiang et al. 2015; Venemans et al. 2015; Bañados et al. 2014; Matsuoka et al. 2016), and the SMBH mass is also comparable to the highest value found in the local universe (McConnell et al. 2011; Thomas et al. 2016). It demonstrates that such a rare, $10^{10} M_{\odot}$ SMBH can be formed as early as $z \gtrsim 6.3$, when the age of the universe was only 890 Myr.

Recent submillimeter and millimeter [(sub)mm] surveys detected strong far-infrared (FIR) continuum, molecular CO, and [C II] $158 \mu\text{m}$ fine structure line emission in the host galaxies of a number of quasars at $z > 5.7$ (e.g., Bertoldi et al. 2003; Priddey et al. 2003; Robson et al. 2004; Walter et al. 2004; Carilli et al. 2007; Wang et al. 2010, 2013; Omont et al. 2013; Willott et al. 2015; Venemans et al. 2016). The results argue for significant host galaxy evolution with active star formation in these young quasars in the early universe, and the [C II] line images at sub-second resolution constrain radius of the nuclear starburst region to be a few kpc (Leipski et al. 2013; Wang et al. 2013; Venemans et al. 2016). The gas dynamics measured with the CO and [C II] observations suggest SMBH-host mass ratios a factor of a few to one order of magnitude higher than the present-day value (Walter et al. 2004; Wang et al. 2013; Willott et al. 2015; Venemans et al. 2016).

The most massive $z > 6$ quasar-galaxy systems studied in previous millimeter and ra-

radio observations are objects with SMBH masses of a few $10^9 M_\odot$ and $L_{\text{bol}} \lesssim 10^{14} L_\odot$ (e.g., Wang et al. 2013; Willott et al. 2015; Venemans et al. 2016). The discovery of J0100+2802 provides a unique chance to study the quasar-galaxy co-evolution in the system that hosts the most massive known SMBH at the earliest epoch. In this work, we report our new observations of the (sub)mm and radio continuum, [C II] $158\mu\text{m}$, and molecular CO lines from the host galaxy of J0100+2802. The observations are described in Section 2, the results are presented in Section 3. We discuss the quasar spectral energy distribution (SED), FIR continuum, [C II], and CO line ratios, and constraints of the host galaxy dynamical mass in Section 4, and summarize the results in Section 5. A Λ -CDM cosmology with $H_0 = 71 \text{ km s}^{-1} \text{ Mpc}^{-1}$, $\Omega_M = 0.27$ and $\Omega_\Lambda = 0.73$ is adopted throughout this paper (Spergel et al. 2007).

2. Observations

2.1. PdBI observations

We observed the [C II] $158\mu\text{m}$ (${}^2\text{P}_{3/2} - {}^2\text{P}_{1/2}$) and molecular CO(6-5) line emission from J0100+2802 using the Plateau de Bure interferometer (PdBI). The observations were carried out in Summer 2014 in D-configuration using five antennas. We used the WideX wide-band correlator in dual polarization with a total bandwidth of 3.6GHz. We set up the correlator centered at the frequency of 260.35 GHz for the [C II] line and 94.72 GHz for the CO(6-5) line. This corresponds to the quasar Mg II line redshift of $z=6.30$ (Wu et al. 2015). The flux density scale was determined based on observations of the standard flux density calibrator MWC349, and the typical calibration uncertainties are 10% at 3 mm and 20% at 1 mm. The phase was checked about every 22min by observing a nearby phase calibrator, J0112+321. We reduced the data using the Grenoble Image and Line Data Analysis System (GILDAS) software (Guilloteau & Lucas 2000). The maps were made using natural weighting. The FWHM synthesized beam sizes are $2.00'' \times 1.66''$ and $5.41'' \times 4.31''$ at the [C II] and CO(6-5) frequencies, respectively. The final rms sensitivity of the [C II] line observation is $2.3 \text{ mJy beam}^{-1}$ per 46 km s^{-1} channel with a total on-source integration time of 4.5 hours, and the rms of the CO(6-5) observation is $0.42 \text{ mJy beam}^{-1}$ per 63 km s^{-1} channel in 13.2 hours.

2.2. VLA observations

We observed the CO(2-1) line emission with the Karl G. Jansky Very Large Array (VLA) in Ka-Band ($\sim 32 \text{ GHz}$) in C-configuration in Oct-Nov 2014, and the 3 GHz radio continuum in S-band in A-configuration in June 2015. The observations were performed

using the WIDAR correlator with the 8-bit sampler in dual polarization. The setup covers a total bandwidth of 2 GHz with sixteen 128 MHz spectral windows and the channel width in each spectral window is 2 MHz. We have spent a total on-source observing time of 7.2 hours for the CO(2-1) line observation and 2.1 hours for the 3 GHz continuum. The flux density calibration was carried out using the standard VLA calibrator 3C48 with typical calibration uncertainties better than 5%. The phases were checked with nearby point sources.

We reduced the data using the Common Astronomy Software Applications package (CASA v4.4) and the VLA calibration pipeline version 1.3.4. The FWHM synthesized beam size is $0.74'' \times 0.68''$ at 32 GHz and $0.65'' \times 0.54''$ at 3 GHz, using robust weighting. For the CO(2-1) line observations, we binned the data to a channel width of 57 km s^{-1} , and obtained a typical 1σ rms noise of $0.067 \text{ mJy beam}^{-1}$ per channel. The channels affected by radio frequency interference were removed in the S-Band observations, resulting in a useful frequency range of ~ 2.4 to 4 GHz and bandwidth of about 1.6 GHz. The final continuum sensitivity at 3 GHz was $3.1 \mu\text{Jy beam}^{-1}$.

2.3. SCUBA-2 observations

We observed the $450\mu\text{m}$ (666 GHz) and $850\mu\text{m}$ (353 GHz) dust continuum from J0100+2802 using the Submillimetre Common-User Bolometer Array 2 (SCUBA-2, Holland et al. 2013) on the James Clerk Maxwell Telescope (JCMT) in Nov 2015. The observations were carried out in Band 2 weather conditions (i.e. $0.05 < \tau_{225\text{GHz}} < 0.008$), and in 'CV DAISY' mode which is designed for point/compact source observations. The beam size of SCUBA-2 is $7.9''$ at 666 GHz and $13''$ at 353 GHz. We observed the target in four 30min scans with a total on-source time of ~ 2 hours. The data was reduced using the STARLINK SCUBA-2 pipeline for faint point sources (Chapin et al. 2013), and we obtained a 1σ point-source sensitivity of 1.2 mJy at 353 GHz and 10 mJy at 666 GHz.

3. Results

We summarize the measurements of redshift, line flux, FWHM line width, and luminosity of the [C II], CO(6-5), and CO(2-1) lines, as well as the continuum in Table 1. The [C II] and CO(6-5) lines are clearly detected (Figure 1), as well as the continuum emission at 353 GHz, 260 GHz, and 3 GHz. We fit a Gaussian line profile to the [C II] and CO(6-5) line spectra to determine the redshifts and line widths, and integrate the continuum-subtracted data over the line-emitting channels to get the line flux. The redshifts and line widths

measured on the [C II] and CO(6-5) lines are consistent with each other within the errors, and we adopt $z_{[\text{CII}]} = 6.3258 \pm 0.0010$ as the redshift of the quasar host galaxy. We obtain tentative detections for the CO(2-1) line and the 32 GHz continuum. The central frequency and width of the CO(2-1) line are difficult to constrain due to the poor signal to noise ratio (SNR) of the spectrum. We integrate the visibility data over the velocity range of the CO(6-5) line emission (i.e., 800 km s^{-1} to 1300 km s^{-1} in Figure 1), and the intensity map shows a 3.6σ peak about $0.27''$ away from the optical quasar position. Considering the measurement uncertainties and the astrometric mismatch between radio and optical frame, this is consistent with the quasar optical position. We also measure the 32 GHz continuum emission to be $S_{32\text{GHz}} = 14.8 \pm 4.3 \mu\text{Jy}$ by averaging all the line-free spectral windows. We subtract the continuum from the line-emitting channels, resulting in a CO(2-1) line flux of $0.038 \pm 0.013 \text{ Jy km s}^{-1}$ at the peak position. Due to the poor SNR of the intensity map, we cannot obtain reliable measurement of the source size, or address if there are more extended components with lower surface brightness.

The quasar Mg II line emission from J0100+2802 measures a redshift of $z_{\text{MgII}} = 6.301 \pm 0.006$ (Figure 3 in Wu et al. 2015), which is blueshifted by $1020 \pm 250 \text{ km s}^{-1}$ compared to $z_{[\text{CII}]}$. Similar blueshifted Mg II lines with velocity offsets of a few hundred to 1700 km s^{-1} are also detected in several other $z > 6$ quasars (Willott et al. 2015; Venemans et al. 2016). Such large Mg II line velocity offsets with respect to the quasar host galaxy redshift are rare at low redshift (Richards et al. 2002), and may suggest outflowing gas in the broad line region at an early evolutionary phase. A larger sample of high- z quasars with z_{MgII} and $z_{[\text{CII}]}$ measurements is required to investigate the relationship between MgII velocity offset and quasar luminosities (Venemans et al. 2016) and address the origin of the blueshifted quasar Mg II line.

4. Discussion

4.1. Continuum emission and spectral energy distribution

The new observations we present here measure the rest-frame FIR to radio continuum emission from J0100+2802. We plot the SED of J0100+2802 in Figure 2 (Wu et al. 2015), together with the data from SDSS, the Two Micron All Sky Survey (2MASS), and the Wide-field Infrared Survey Explorer (WISE). The templates of optically luminous quasars from Elvis et al. (1994) and Richards et al. (2006) are also plotted for comparison. We scale the templates to the 2MASS H-band flux, and the (sub)mm measurements show no excess compared to the FIR emission of the scaled templates. We cannot rule out that the FIR continuum emission from J0100+2802 is dominated by thermal emission from the AGN-heated

dust. However, the detections of [C II] and CO line emission do argue for star forming interstellar medium (ISM) in the nuclear region (see Section 4.2). We fit the (sub)mm flux densities to an optically thin graybody model with a dust temperature of $T_{\text{dust}} = 47$ K and an emissivity index of $\beta = 1.6$ from the (sub)mm-detected quasars at $z > 1.7$ (Beelen et al. 2006). This results in a FIR ($42.5\mu\text{m}$ - $122.5\mu\text{m}$) luminosity of $L_{\text{FIR}} = (3.5 \pm 0.7) \times 10^{12} L_{\odot}$, and a $8\mu\text{m}$ - $1000\mu\text{m}$ IR luminosity of $L_{\text{IR}} = (5.0 \pm 0.9) \times 10^{12} L_{\odot}$. The star formation rate (SFR) estimated with the IR luminosity using the relation in Kennicutt (1998) is $850 M_{\odot} \text{ yr}^{-1}$. As the fraction contributed from the torus is unknown, this constrains the upper limits of the star formation-powered FIR emission and SFR in the host galaxy. The dust mass calculated based on the above dust temperature and emissivity index assumption is $M_{\text{dust}} = (2.0 \pm 0.4) \times 10^8 M_{\odot}$. We adopt a dust absorption coefficient of $\kappa_{\text{d}}(\lambda) \sim \lambda^{-\beta}$ and $\kappa_{\text{d}}(125\mu\text{m}) = 18.75 \text{ cm}^2 \text{ g}^{-1}$ (Hildebrand 1983) in the calculation. If a higher dust temperature of 60 K is adopted (i.e., the highest temperature seen among the submillimeter/millimeter-detected $z \sim 6$ quasars, Leipski et al. 2013), the FIR luminosity and SFR increase by a factor of 1.7, and the dust mass will decrease by a factor of 1.8. If we adopt the lowest dust temperature of 40 K found by Leipski et al. (2013), the FIR and SFR will decrease by a factor of 1.5, and the dust mass increases by a factor of 1.6 (Table 1).

The VLA Ka and S-band observations measure the rest-frame 234 GHz and 22 GHz continuum emission, respectively. The corresponding continuum luminosities are $\nu L_{\nu, 234\text{GHz}} = (5.8 \pm 1.7) \times 10^8 L_{\odot}$ and $\nu L_{\nu, 22\text{GHz}} = (3.9 \pm 0.1) \times 10^8 L_{\odot}$. We calculate the radio loudness of this object adopting the definition of $R = f_{\nu, 5\text{GHz}} / f_{\nu, 4400\text{\AA}}$ (Kellermann et al. 1989). The rest-frame 4400Å flux density ($f_{\nu, 4400\text{\AA}}$) is interpolated using the scaled Richards et al. (2006) optically luminous quasar template (Figure 1), and the rest-frame 5 GHz flux density ($f_{\nu, 5\text{GHz}}$) is extrapolated from 22 GHz data assuming a power-law radio continuum of $f_{\nu} \propto \nu^{\alpha}$. This constrains the radio loudness to be $R = 0.9$ for a steep spectrum of $\alpha = -0.9$, or $R = 0.2$ for a flat spectrum of $\alpha = -0.06$ (see below for the discussion of spectral index), indicating that this object is radio quiet. However, the 234 GHz and 22 GHz luminosities are more than an order of magnitude higher than the thermal bremsstrahlung or nonthermal synchrotron continuum expected from star forming activities (e.g., Condon 1992; Yun et al. 2000; Yun & Carilli 2002; Zakamska et al. 2016). For instance, the thermal bremsstrahlung or nonthermal synchrotron continuum estimated with a SFR of $850 M_{\odot} \text{ yr}^{-1}$ using the formulae in Yun & Carilli (2002) contributes $< 5\%$ of the detected continuum emission at both frequencies. Additionally, the thermal dust emission has only a minor contribution of 12% to 21% to the 234 GHz flux density based on the graybody models with $T_{\text{dust}} = 60$ K to 40 K described above. Thus, the continuum emission in J0100+2802 at frequencies of 234 GHz and lower is dominated by the radio activity of the central AGN.

In Figure 1, we adopt the graybody model with $T_{\text{dust}} = 47$ K to remove the dust con-

tinuum at 234 GHz and fit a power-law ($f_\nu \sim \nu^\alpha$) to the remaining 234 GHz flux density and the 22 GHz data. This estimates the 234-to-22 GHz two-point spectral index to be $\alpha_{22\text{GHz}}^{234\text{GHz}} = -0.90 \pm 0.15$. We also measure the spectral index within the S-band by averaging the data in every two 128MHz spectral windows from the observed frequencies of 2.4 GHz to 4 GHz. In contrast to the steep spectrum indicate by $\alpha_{22\text{GHz}}^{234\text{GHz}}$, the best result fit to the seven data points in S-band yield a flat spectrum with $\alpha_{22\text{GHz}} = -0.06 \pm 0.22$. J0100+2802 provides a great example to study the radio activity in the most optically luminous and radio quiet nucleus at the earliest epoch. We will need further observations at multiple radio frequencies to check if the radio continuum is indeed flattened or inverse around 22 GHz. Additionally, milli-arcsecond resolution observations through Very Long Baseline Interferometry are needed to measure the spatial extent of the radio source in this object and address if there are multiple components contribute to the detected radio continuum as was widely discussed in the radio quiet quasars at lower redshift (e.g., Ulvestad et al. 1999, 2005)

4.2. Luminosity ratios and gas masses

Based on the FIR luminosity driven in the previous section, we constrain the [C II]-to-FIR luminosity ratio to be 0.0010 ± 0.0002 . This is comparable to the values found in other [C II]-detected $z > 5.7$ quasars that have similar moderate FIR luminosities of $L_{\text{FIR}} \lesssim 1 \times 10^{12} L_\odot$ to $\sim 4 \times 10^{12} L_\odot$, and higher than that from the more FIR luminous objects ($L_{\text{FIR}} \geq 5 \times 10^{12} L_\odot$, Wang et al. 2013), i.e., following the trend of decreasing FIR luminosity with increasing [C II]-to-FIR luminosity ratios defined by the high-redshift quasars and starburst galaxies (Maiolino et al. 2009; Riechers et al. 2013; De Breuck et al. 2014; Willott et al. 2015; Gullberg et al. 2015; Venemans et al. 2016; Muñoz & Oh 2015; Narayanan & Krumholz 2016). The SFR estimated with the [C II] luminosity is $560 M_\odot \text{ yr}^{-1}$, adopting the SFR-[C II] luminosity relation for high-redshift galaxies in De Looze et al. (2014). This is consistent with the SFR estimates based-on the dust continuum.

The CO observations measure a CO (6-5)-to-(2-1) line flux ratio of 8.4 ± 3.6 and a line luminosity ratio of $L'_{\text{CO}(6-5)}/L'_{\text{CO}(2-1)} = 0.94 \pm 0.40$. This is consistent with the ratios found in other CO-detected $z > 5.7$ quasars within the errors (Wang et al. 2011; Stefan et al. 2015), suggesting that the detected CO emission is likely from a highly-excited molecular gas component peaked at $J=6$ or higher (Riechers et al. 2009; Gallerani et al. 2014; Stefan et al. 2015). If we assume that the low- J CO transitions are thermalized, i.e., $L'_{\text{CO}(1-0)} = L'_{\text{CO}(2-1)}$ (e.g., Carilli & Walter 2013), and adopt a luminosity-to-mass conversion factor of $\alpha_{\text{CO}} = 0.8 M_\odot / \text{K km s}^{-1} \text{ pc}^2$ from the local ultraluminous infrared galaxies (Downes & Solomon 1998), the detected CO(2-1) line flux yields a molecular gas mass of $M_{\text{mol}} = (1.0 \pm 0.3) \times 10^{10} M_\odot$.

However, the total molecular gas mass in the quasar host could be larger considering that some of the CO (2-1) line flux from the low surface brightness region and the line wings might be missing due to the poor SNR of the observation.

We compare the luminosity ratios of the FIR continuum, [C II], and CO lines from J0100+2802 to the models of Photo dissociation region (PDR¹, Kaufman et al. 1999, 2006; Pound & Wolfire 2008) in Figure 3, to investigate the gas density n and the incident far-ultraviolet radiation field G_0 (in units of the Habing Field, $1.6 \times 10^{-3} \text{ ergs cm}^{-2} \text{ s}^{-1}$) of the interstellar medium in the quasar host galaxy. As a one-side illuminated slab geometry was adopted in the model, we here divide the optically thin FIR² and [C II] line emission by a factor of 2 to match the condition in the model. We also multiply $L_{[\text{C II}]}$ by a factor of 0.7 to estimate and exclude the [C II] emission from the diffuse region (Stacey et al. 1991; Colbert et al. 1999). According to Figure 3, the overlap region of the three luminosity ratios suggests G_0 of a few thousand and $n \gtrsim 1 \times 10^5 \text{ cm}^{-3}$. These are only preliminary constraints on the physical condition of the star forming region in the host galaxy of J0100+2802. There are still large uncertainties in the calculation of FIR luminosity. The fractions of [C II] and CO emission from the PDR region are also not well determined. A larger FIR luminosity with a higher T_{dust} will result in a higher G_0 , and any contribution from the X-ray dominated regions (XDR) to the detected CO (6-5) line emission (e.g., Gallerani et al. 2014) will result in a higher $L_{[\text{C II}]} / L_{\text{CO}(6-5)}$ and a lower $L_{\text{CO}(6-5)} / L_{\text{CO}(2-1)}$ from the PDR region and move the best-fit gas density to $n < 10^5 \text{ cm}^{-3}$.

We estimate the atomic gas mass within the PDR region from the [C II] line luminosity using Equation (1) in Hailey-Dunsheath et al. (2010), adopting the best fit parameters indicated in Figure 3 (i.e., $G_0 \sim 4000$, $n \sim 10^{5.1} \text{ cm}^{-3}$, and a corresponding PDR surface temperature of $T \sim 550 \text{ K}$, Kaufman et al. 1999), a C^+ abundance of 1.4×10^{-4} , and a critical density of $n_{\text{crit}} = 2.7 \times 10^3 \text{ cm}^{-3}$. The derived atomic gas mass in the PDR region is $M_{\text{atomic,PDR}} \sim 3 \times 10^9 M_{\odot}$, which is about 30% of the molecular gas mass estimated with the CO (2-1) line. The mass ratio associated with the detected CO, [C II], and FIR dust emission is $(M_{\text{mol}} + M_{\text{atomic,PDR}}) / M_{\text{dust}} \sim 65$. This is comparable to the mass ratios of other CO-detected quasars and dusty starburst galaxies at high- z (Wang et al. 2010; Michalowski et al. 2010; Riechers et al. 2013).

¹The line and FIR ratio models are taken from the Photo Dissociation Region Toolbox (<http://dustem.astro.umd.edu/pdrt/>).

²The FIR luminosity is re-calculated in the range of $30\mu\text{m}$ to $1000\mu\text{m}$ to match the definition in the models.

4.3. Constraint on host galaxy dynamical mass

Among the quasars known at $z > 6$, J0100+2802 has the most massive SMBH with a mass of $(1.24 \pm 0.19) \times 10^{10} M_{\odot}$ (Wu et al. 2015; De Rosa et al. 2011). We use the [C II] line width ($\text{FWHM}_{[\text{C II}]}$) to present a preliminary estimate of the host galaxy mass for this object. We assume that the line is from a rotating gas disk and the circular velocity can be estimated as $v_{\text{cir}} = 0.75 \text{FWHM}_{[\text{C II}]} / \sin(i)$, where i is the inclination angle between the rotation axis of the disk and the line of sight. The [C II] line emission from J0100+2802 is unresolved in our PdBI observation at $2''$ resolution. According to the recent [C II] observations of other $z \sim 6$ quasars at sub-arcsecond resolution, the typical FWHM major axis sizes of the [C II] emission are about $2 \sim 4$ kpc (Wang et al. 2013; Willott et al. 2013, 2015; Venemans et al. 2016). Thus, we here estimate the FWHM [C II] source size for J0100+2802 to be 3 ± 1 kpc (see also Willott et al. 2015; Venemans et al. 2016) and set the diameter of the gas disk D as $1.5 \times$ the FWHM [C II] source size, i.e., $D = 4.5 \pm 1.5$ kpc. The host galaxy dynamical mass is then $M_{\text{dyn}}(M_{\odot}) = 1.16 \times 10^5 v_{\text{cir}}^2 D = [2.6(D/4.5 \text{ kpc}) \pm 1.6] \times 10^{10} / \sin^2(i) M_{\odot}$. The error includes the uncertainties from both the line width and the assumed disk size.

We plot M_{BH} vs. M_{dyn} for J0100+2802 and other $z > 5.7$ quasars in Figure 4 (Wang et al. 2013; Willott et al. 2013, 2015; Bañados et al. 2015; Venemans et al. 2016), comparing to the SMBH-to-bulge mass relation of local galaxies from Kormendy & Ho (2013), i.e., $M_{\text{BH}} / (10^9 M_{\odot}) = 0.49 (M_{\text{bulge}} / 10^{11} M_{\odot})^{1.16}$. For J0100+2802 as well as other $z > 5.7$ quasars that have SMBH mass measurements based on the quasar Mg II line emission (De Rosa et al. 2011, 2014; Willott et al. 2013, 2015), we follow Willott et al. (2015) and add a 0.3 dex uncertainty to the error bar of the SMBH mass to account for the scatter of the calibration (Shen et al. 2008). For the sample from Wang et al. (2013) which do not have SMBH mass measurements, we adopt the relationship between the 1450 \AA luminosity and the quasar bolometric luminosity from Venemans et al. (2016), and calculate the Eddington luminosities and SMBH masses assuming a typical Eddington ratio and a scatter of $\log(L_{\text{bol}}/L_{\text{Edd}}) = -0.3 \pm 0.3$ from De Rosa et al. (2011). The M_{dyn} for most of the $z > 5.7$ quasars are estimated based on [C II] observations (Wang et al. 2013; Willott et al. 2013, 2015; Bañados et al. 2015; Venemans et al. 2016). The only exception is the $z = 6.42$ quasar SDSS J114816.64+525150.3, in which the [C II]-emitting gas at > 1.5 kpc scale is turbulent (Cicone et al. 2015) and the CO size is used (Riechers et al. 2009; Stefan et al. 2015) in the M_{dyn} calculation. According to Figure 4, for any inclination angle of $i \geq 10^\circ$, J0100+2802 is above the local $M_{\text{BH}} - M_{\text{bulge}}$ relation and the ± 0.3 dex area of the intrinsic scatter (i.e. the gray area in Figure 3). As was discussed in Willott et al. (2015), most of the $z \sim 6$ quasars with SMBH masses on order of $10^8 M_{\odot}$ are close to the trend of local galaxies, while the more luminous and massive objects tend to be above this trend (see also Venemans et al. 2016). This suggests that the SMBH grows faster than the quasar host galaxies in these most massive systems at the earliest

epoch, unless all these $M_{\text{BH}} > 10^9 M_{\odot}$ quasars are close to face-on. However, as there is no resolved image for J0100+2802 yet, we do not rule out the possibility that the gas is unvirialized and the [C II] line width cannot probe the disk circular velocity.

5. Summary

We detected [C II], CO, and (sub)mm and radio continuum emission in the host galaxy of the quasar J0100+2802 which hosts the most massive SMBH known at $z \geq 6$. The detections probe the properties of the young quasar host at an early evolutionary stage: The (sub)mm continuum indicates moderate FIR emission and constrains the SFR to be $\leq 850 M_{\odot} \text{ yr}^{-1}$. The CO and [C II] lines estimate the gas mass and gas-to-dust mass ratio that are within the range of other millimeter-detected quasars at $z \sim 6$. The [C II]-to-FIR luminosity ratio J0100+2802 is higher than that of the most FIR luminous quasars at $z > 5.7$, i.e., following the trend of increasing $L_{[\text{C II}]} / L_{\text{FIR}}$ with decreasing L_{FIR} found with the high- z quasars and star forming systems. The quasar Mg II line emission detected in previous near-infrared spectroscopic observation (Wu et al. 2015) is blueshifted by about 1000 km s^{-1} compared to the host galaxy redshift measured by the [C II] and CO lines. The host dynamical mass estimated with the [C II] line width suggest that the SMBH is likely to be overmassive, compared to the local relation, though further constraints on the gas kinematics and disk inclination angle are still required.

The data presented in this paper are based on observations under project number S14CY with the IRAM Plateau de Bure Interferometer, projects 14B151 and 15A494 with the VLA, and project M15BI055 with JCMT/SCUBA-2. IRAM is supported by INSU/CNRS (France), MPG (Germany) and IGN (Spain). The National Radio Astronomy Observatory is a facility of the National Science Foundation operated under cooperative agreement by Associated Universities, Inc. The James Clerk Maxwell Telescope is operated by the East Asian Observatory on behalf of The National Astronomical Observatory of Japan, Academia Sinica Institute of Astronomy and Astrophysics, the Korea Astronomy and Space Science Institute, the National Astronomical Observatories of China and the Chinese Academy of Sciences (Grant No. XDB09000000), with additional funding support from the Science and Technology Facilities Council of the United Kingdom and participating universities in the United Kingdom and Canada. We are thankful for the supports from the National Science Foundation of China (NSFC) grants No.11373008, 11533001, the Strategic Priority Research Program "The Emergence of Cosmological Structures" of the Chinese Academy of Sciences, grant No. XDB09000000, the National Key Basic Research Program of China 2014CB845700, the Ministry of Science and Technology of China under grant 2016YFA0400703. RW acknowl-

edge supports from the Thousand Youth Talents Program of China, the NSFC grants No. 11443002 and 11473004. XF acknowledge supports from NSF Grants AST 11-07682 and 15-15115. We thank M. Wolfire for providing line ratio maps used in the PDRToolBox.

Facilities: IRAM (PdBI), VLA, JCMT (SCUBA-2).

REFERENCES

- Bañados, E., Venemans, B. P., Morganson, E. et al. 2014, *AJ*, 148, 14
- Bañados, E., Decarli, R., Walter, F., et al. 2015, *ApJL*, 805, 8
- Beelen, A., Cox, P., Bertoldi, F. et al. 2006, *ApJ*, 642, 694
- Bertoldi, F., Cox, P., Neri, R. et al. 2003, *A&A*, 409, L47
- Carilli, C. L., Neri, R., Wang, R. et al. 2007, *ApJ*, 666, L9
- Carilli, C. L. & Walter, F. 2013, *ARA&A*, 51, 105
- Cicone, C., Maiolino, R., Gallerani, S., et al. 2015, *A&A*, 574, 14
- Chapin, E. L., Berry, D. S., Gibb, A. G. et al. 2013, *MNRAS*, 430, 2545
- Colbert, J. W., et al. 1999, *ApJ*, 511, 721
- Condon, J. J. 1992, *ARA&A*, 30, 575
- De Breuck, C., Williams, R. J., Swinbank, M. et al. 2014, *A&A*, 565, 59
- De Looze, I., Cormier, D., Lebouteiller, V. et al. 2014, *A&A*, 568, 62
- De Rosa, G., Venemans, B. P., Decarli, R. et al. 2014, *ApJ*, 790, 145
- De Rosa, G., Decarli, R., Walter, F. et al. 2011, *ApJ*, 739, 56
- Downes, D., & Solomon, P. M. 1998, *ApJ*, 507, 615
- Elvis, M., Wilkes, B. J., McDowell, J. C. et al. 1994, *ApJS*, 95, 1
- Fan, X., Strauss, M. A., Richards, G. T. et al. 2006, *AJ*, 131, 1203
- Gallerani, S., Ferrara, A., Neri, R., & Maiolino, R. 2014, *MNRAS*, 445, 2848
- Guilloteau, S., & Lucas, R. 2000, *ASPC*, 217, 299

- Gullberg, B., De Breuck, C., Vieira, J. D. et al. 2015, MNRAS, 449, 2883
- Hailey-Dunsheath, S., Nikola, T., Stacey, G. J. et al. 2010, ApJ, 714, L162
- Hildebrand, R. H. 1983, QJRAS, 24, 267
- Holland, W. S., Bintley, D., Chapin, E. L. et al. 2013, MNRAS, 430, 2513
- Jiang, L., McGreer, I. D., Fan, X. et al. 2015, AJ, 149, 188
- Leipski, C., Meisenheimer, K., Walter, F. et al. 2013, ApJL, 772, 103
- Kaufman, M. J., Wolfire, M. G., Hollenbach, D. J., & Luhman, M. L. 1999, ApJ, 527, 795
- Kaufman, M. J., Wolfire, M. G., Hollenbach, D. J. 2006, ApJ, 644, 283
- Kennicutt, R. C., Jr. 1998, ARA&A, 36, 189
- Kellermann, K. I., Sramek, R., Schmidt, M., Shaffer, D. B., & Green, R. 1989, AJ, 98, 1195
- Kormendy, J., & Ho, L. C. 2013, ARA&A, 51, 511
- Maiolino, R., Caselli, P., Nagao, T. et al. 2009, A&A, 500, L1
- Matsuoka, Y., Onoue, M., Kashikawa, N. et al. 2016, ApJ, submitted, arXiv:1603.02281
- McConnell, N. J., Ma, C.-P., Gebhardt, K. et al. 2011, Nature, 480, 215
- Michalowski, M. J., Watson, D., & Hjorth, J. 2010, ApJ, 712, 942
- Muñoz, J. A., & Oh, S. P. 2015, MNRAS, submitted, arXiv:1510.00397
- Narayanan, D., & Krumholz, M. 2016, MNRAS, submitted, arXiv:1601.05803
- Omont, A., Willott, C. J., Beelen, A. et al. 2013, A&A, 552, 43
- Petric, A. O., Carilli, C. L., Bertoldi, F. et al. 2003, AJ, 126, 15
- Pound, M. W., & Wolfire, M. G. 2008, ASPC, 394, 654
- Priddey, R. S., Isaak, K. G., McMahon, R. G. et al. 2003, MNRAS, 339, 1183
- Richards, G. T., Vanden Berk, D. E., Reichard, T. A., et al. 2002, AJ, 124, 1
- Richards, G. T., Lacy, M., Storrie-Lombardi, L. J. et al. 2006, ApJS, 166, 470
- Riechers, D. A., Walter, F., Bertoldi, F. et al. 2009, ApJ, 703, 1338

- Riechers, D. A., Bradford, C. M., Clements, D. L. et al. 2013, *Nature*, 496, 329
- Robson, I., Priddey, R. S., Isaak, K. G. et al. 2004, *MNRAS*, 351, L29
- Shen, Y., Greene, J. E., Strauss, M. A., Richards, G. T., & Schneider, D. P. 2008, *ApJ*, 680, 169
- Solomon, P. M., & Vanden Bout, P. A. 2005, *ARA&A*, 43, 677
- Spergel, D. N., Bean, R., Doré, O. et al. 2007, *ApJS*, 170, 377
- Stacey, G. J., Geis, N., Genzel, R., Lugten, J. B., Poglitsch, A., Sternberg, A., & Townes, C. H. 1991, *ApJ*, 373, 423
- Stefan, I. I., Carilli, Chris L., Wagg, J. et al. 2015, *MNRAS*, 451, 1713
- Thomas, J., Ma, Ch.-P., McConnell, N. J. et al. 2016, *Nature*, 532, 340
- Ulvestad, J. S., Wrobel, J. M., Carilli, C. L. 1999, *ApJ*, 516, 127
- Ulvestad, J. S., Antonucci, R. R. J., & Barvainis, R. 2005, *ApJ*, 621, 123
- Venemans, B. P., Bañados, E., Decarli, R. 2015, *ApJ*, 801, L11
- Venemans, B. P., Walter, F., Zschaechner, L. et al. 2016, *ApJ*, 816, 37
- Walter, F., Carilli, C. L., Bertoldi, F. et al. 2004, *ApJ*, 615, L17
- Wang, R., Carilli, C., Neri, R. et al. 2010, *ApJ*, 714, 699
- Wang, R., Wagg, J., Carilli, C., et al. 2011, *ApJ*, 739, L34
- Wang, R., Wagg, J., Carilli, C. et al. 2013, *ApJ*, 773, 44
- Willott, C. J., Delorme, P., Reylé, C. et al. 2010, *AJ*, 139, 906
- Willott, C. J., Omont, A., & Bergeron, J. 2013, *ApJ*, 770, 13
- Willott, C. J., Bergeron, J. & Omont, A. 2015, *ApJ*, 801, 123
- Wu, X.-B., Wang, F., Fan, X. et al. 2015, *Nature*, 518, 512
- Yun, M. S., Carilli, C. L., Kawabe, R. et al. 2000, *ApJ*, 528, 171
- Yun, M. S. & Carilli, C. L. 2002, *ApJ*, 568, 88
- Zakamska, N. L., Lampayan, K., Petric, A. et al. 2016, *MNRAS*, 455, 4191

Table 1: Line and continuum properties of J0100+2802

[C II] redshift	6.3258±0.0010
[C II] FWHM ($km s^{-1}$)	300±77
[C II] line flux ($Jy km s^{-1}$)	3.36±0.46
[C II] line luminosity:	
(L_{\odot})	$(3.56 \pm 0.49) \times 10^9$
($K km s^{-1} pc^2$)	$(1.62 \pm 0.22) \times 10^{10}$
CO(6-5) redshift	6.3264±0.0024
CO(6-5) FWHM ($km s^{-1}$)	498±225
CO(6-5) line flux ($Jy km s^{-1}$)	0.32±0.084
CO(6-5) line luminosity:	
(L_{\odot})	$(1.23 \pm 0.32) \times 10^8$
($K km s^{-1} pc^2$)	$(1.17 \pm 0.30) \times 10^{10}$
CO(2-1) line flux ($Jy km s^{-1}$)	0.038±0.013
CO(2-1) line luminosity:	
(L_{\odot})	$(4.89 \pm 1.67) \times 10^6$
($K km s^{-1} pc^2$)	$(1.25 \pm 0.43) \times 10^{10}$
CO(1-0) line luminosity [derived from the CO (2-1) line]:	
(L_{\odot})	$(6.11 \pm 2.09) \times 10^5$
($K km s^{-1} pc^2$)	$(1.25 \pm 0.43) \times 10^{10}$
666 GHz continuum (mJy)	<30
353 GHz continuum (mJy)	4.1±1.2
260 GHz continuum (mJy)	1.35±0.25
94.5 GHz continuum (mJy)	<0.1
32 GHz continuum (μ Jy)	14.8±4.3
3 GHz continuum (μ Jy)	104.5±3.1
FIR luminosity (L_{\odot}):	
$T_{dust} = 47 K, \beta = 1.6$	$(3.5 \pm 0.7) \times 10^{12}$
$T_{dust} = 40 K, \beta = 1.6$	$(2.4 \pm 0.5) \times 10^{12}$
$T_{dust} = 60 K, \beta = 1.6$	$(6.0 \pm 1.2) \times 10^{12}$
dust mass (M_{\odot}):	
$T_{dust} = 47 K, \beta = 1.6$	$(2.0 \pm 0.4) \times 10^8$
$T_{dust} = 40 K, \beta = 1.6$	$(3.1 \pm 0.6) \times 10^8$
$T_{dust} = 60 K, \beta = 1.6$	$(1.1 \pm 0.2) \times 10^8$

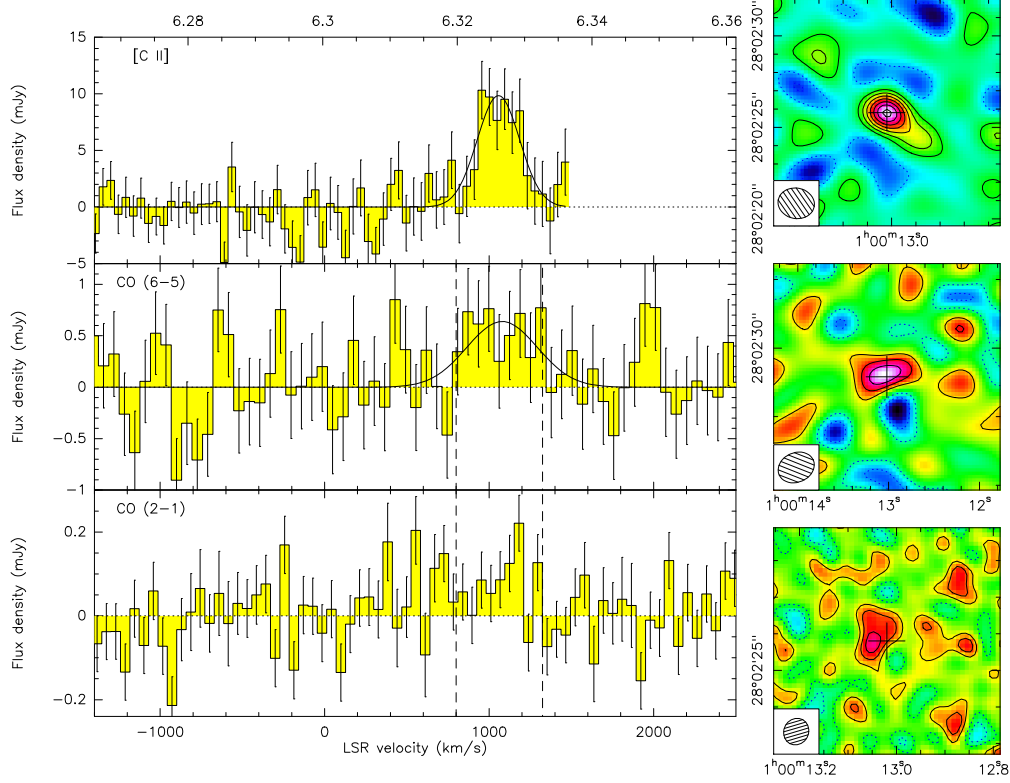


Fig. 1.— The line spectra (left) and velocity integrated map (right) of the [C II] $158\mu\text{m}$ (upper panel), CO(6-5) (middle panel), and CO(2-1) line emission (lower panel) from J0100+2802. The bottom abscissa shows the radio velocity in Kinematic Local Standard of Rest (LSRK) frame, where zero velocity corresponds to $z_{\text{MgII}} = 6.30$ (Wu et al. 2015). The top abscissa denotes the corresponding redshift. The contours for the [C II] line intensity map are $[-2, -1, 1, 2, 3, 4, 5, 6, 7] \times 0.77 \text{ mJy beam}^{-1}$, and $[-2, -1, 1, 2, 3] \times 0.15 \text{ mJy beam}^{-1}$ for the CO (6-5) line. The CO(2-1) line intensity map is obtained by integrating over the velocity range defined by the CO(6-5) line (vertical dashed lines), and contours are $[-2, -1, 1, 2, 3] \times 23 \mu\text{Jy beam}^{-1}$. The cross in each panel denotes the position of the optical quasar, and the synthesized beams are plotted at the bottom left of each map.

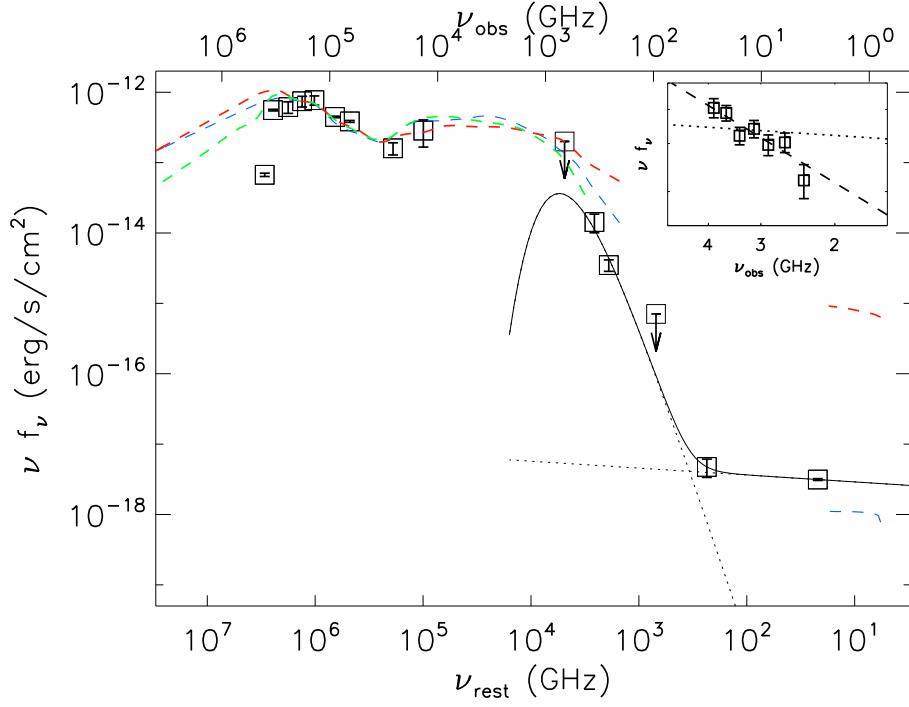


Fig. 2.— The rest-frame UV-to-radio SED of J0100+2802. The squares show the data from SDSS, 2MASS, and WISE (Wu et al. 2015), and the new measurements in this work. The arrows denote 3σ upper limits. The templates of local radio quiet (blue line) and radio loud quasars (red line, Elvis et al. 1994) and SDSS optically luminous quasars (green line, Richards et al. 2006) are plotted and scaled to the 2MASS H-band flux. The dotted lines are the graybody and power-law (with $f_\nu \sim \nu^\alpha$ and $\alpha_{22\text{GHz}}^{234\text{GHz}} = -0.90$) fit to the FIR and radio continuum, respectively, and the black solid line shows the total emission from these two components. The inner panel shows the S-band continuum fluxes measured in every 258 MHz frequency bins from 2.3 to 4 GHz. The dotted line is the power-law with $\alpha_{22\text{GHz}}^{234\text{GHz}} = -0.90$ fitted to the Ka-band continuum and the S-band flux density averaged over the total 1.6 GHz bandwidth, while the dashed line is the best fitting result to only the S-band data with $\alpha_{22\text{GHz}} = -0.06$.

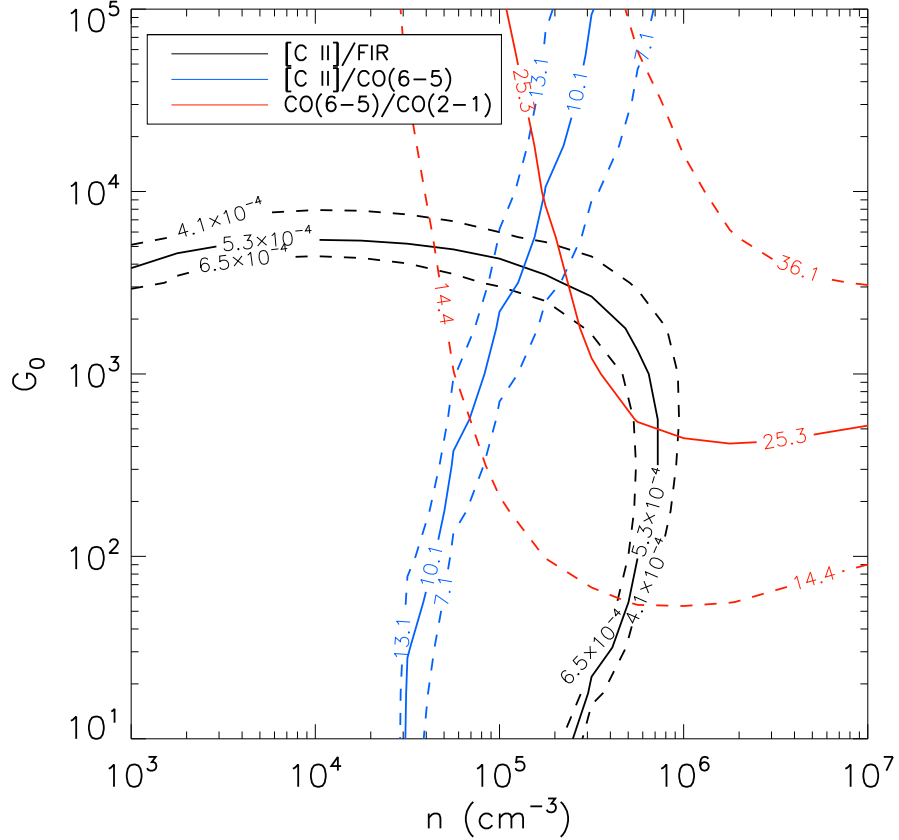


Fig. 3.— Luminosity ratios of $L_{[\text{C II}]} / L_{\text{FIR}}$ (black), $L_{[\text{C II}]} / L_{\text{CO}(6-5)}$ (blue), and $L_{\text{CO}(6-5)} / L_{\text{CO}(2-1)}$ (red) compared to the PDR models of Kaufman et al. (1999) in different conditions of radiation field G_0 and gas density n . Luminosities are all in unit of L_\odot . The dashed contours denote the $\pm 1\sigma$ error bars from the observing uncertainties. We adopt the optically thin graybody model with $T_{\text{dust}} = 47$ K and $\beta = 1.6$ to calculate L_{FIR} . The L_{FIR} here is integrated in the wavelength range of $30\mu\text{m}$ to $1000\mu\text{m}$ to match the FIR definition in the model. We also assume that 70% of the detected [C II] line emission is from the PDR region. Thus the $L_{[\text{C II}]} / L_{\text{FIR}}$ value in the plot is lower than the value of 0.001 quoted in Section 4.1. We also divide $L_{[\text{C II}]}$ and L_{FIR} by a factor of 2 to match the one-side illuminated geometry in the model.

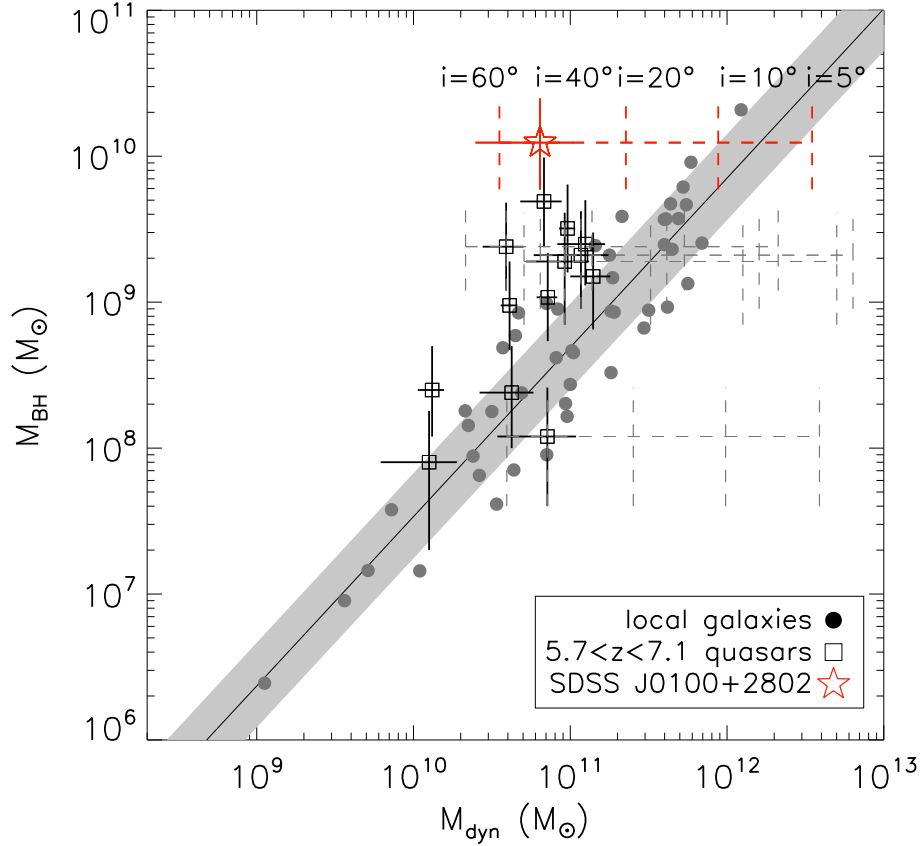


Fig. 4.— M_{BH} vs. M_{dyn} of the [C II]-detected $z > 5.7$ quasars. The M_{dyn} for $z > 5.7$ quasars are estimated based on [C II] observations, except one object, SDSS J114816.64+525150.3 at $z=6.42$, in which the [C II]-emitting gas at >1.5 kpc scale is turbulent and the CO size is adopted (Riechers et al. 2009; Wang et al. 2013; Willott et al. 2013, 2015; Cicone et al. 2015; Venemans et al. 2016). The red star shows J0100+2802 in this work. For objects that do not have an inclination angle estimated with the resolved [C II] image, we show M_{dyn} calculated with different inclination angles (dashed lines). The solid line and the gray region show the local relationship with ± 0.3 dex intrinsic scatter. The gray circles are the sample of local galaxies (Kormendy & Ho 2013).